The Vortical Flow Field of Delta Wing with Leading Edge Extension

Ki Young Lee*, Myong Hwan Sohn

Department of Mechanical Engineering Korea Air Force Academy Chongwon-Gun, Choongbook-Do 363-849, Korea

The interaction and breakdown of vortices over the Leading Edge Extension (LEX)- Delta wing configuration has been investigated through wing-surface pressure measurements, the off-surface flow visualization, and 5-hole probe measurements of the wing wake section. The description focused on analyzing the interaction and the breakdown of vortices depending on the angle of attack and the sideslip angle. The Effect of angle of attack and sideslip angle on the aerodynamic load characteristics of the model is also presented. The sideslip angle was found to be a very influential parameter of the vortex flow over the LEX-delta wing configuration. The introduction of LEX vortex stabilized the vortex flow, and delayed the vortex breakdown up to a higher angle of attack. The vortex interaction and breakdown was promoted on the windward side, whereas it was suppressed on the leeward side.

Key Words : Vortex Interaction, Vortex Breakdown, Flow Visualization, 5-Hole Probe, Sideslip Angle, Leading Edge Extension

1. Introduction

Super-maneuverability is one of the key design parameters for modern and future combat aircraft mission accomplishment. To achieve the desired high degree of fighter maneuverability, the delta wing having the leading edge extension (LEX) or the strake configuration is employed for several modern fighter aircraft such as F-22, F-35. This type of wing geometry is known to be able to improve aerodynamic performance more than the delta wing alone configuration, especially at higher angles of attack (Sohn and Lee, 2002; Chung et al., 2002).

The flow over a LEX/delta wing is complicated because of the additional phenomenon of vortex interaction between the LEX vortex and wing vortex. At low angles of attack, leading edge vortices from both the LEX and wing remain distinctly separate from each other. As the angle of attack increases, the LEX and wing vortices start to interact (Hebber et al., 2000). In Particular, at high angles of attack, the strong LEX vortex induces a lateral velocity field, which energizes the boundary layer above the wing upper surface. This LEX vortex stabilizes the main wing vortices, and delaying its vortex breakdown to a higher angle of attack.

The vortical flow field is influenced by several wing parameters, which include sweep angle, leading edge geometry, as well as free stream conditions and angle of attack. Among these parameters, the sideslip angle makes the vortical flow field of the delta wing at high angle of attack a more complex one. The wing side leading into the flow (the windward side) has an effective increase in sweep angle. The decrease in effective sweep will cause stronger vortices, but it will also increase the likelihood of vortex breakdown (Verhaagen, 1999). Up to now the sideslip angle is known to be the most influential parameter

* Corresponding Author,
E-mail : kylee@afa.ac.kr
TEL : +82-43-290-6472; **FAX** : +82-43-297-6661
Department of Mechanical Engineering Korea Air Force Academy Chongwon-Gun, Choongbook-Do 363-849, Korea. (Manuscript **Received** October 30, 2002; **Revised** March 12, 2003)

causing the asymmetric vortex development and breakdown, and the dynamic stability problem of a sharp-edge delta wing or a highly swept slender wing.

There have been a number of research efforts to examine the performance of LEX/delta wing configuration (Ericksson, 1999 ; Cornelius, 1995 ; Ekaterinaris, 1995 ; Boer and Cunningham, 1990 ; Cunningham and Boer, 1990 ; Fujii and Schiff, 1989 ; Hoeijimarkers and Vaatstra, 1983). However, only a few studies have been performed about the vortex flow over the LEX/delta wing configuration with sideslip (Grismer and Nelson, 1995 ; Verhaagen and Naarding, 1989).

The purpose of this article is to undertake a detailed experimental analysis on the characteristics of vortical flow for the LEX-delta wing configuration with and without sideslip. Vortical flow was studied using off-surface flow visualizations, wing upper surface pressure, and 5-hole probe measurements. A new visualization technique of employing the ultrasonic humidifier water droplet and laser beam sheet was developed and applied to visualize the vigorous vortical regions of the model. The findings of these experimental analyses revealed the interaction and breakdown of vortices depending on angle of attack and sideslip angle. These results expand general knowledge and develop a broad, consistent data base for this type of vortical flow.

2. Experimental Apparatus

2.1 Wind tunnel facilities

Experiments were carried out in two wind tunnel facilities of the Korea Air Force Academy. The measurement of the wing upper surface pressure and the 5-hole probe measurement were carried out in the medium sized low-speed wind tunnel that has a test section of 3.5 m(W) ×2.45 m(H) ×8.7 m(L). The wind tunnel is powered by a 2,100 kW motor that provides a maximum free stream velocity of 92 m/s. The mean intensity of turbulence is 0.034%(u'), and 0.093% (w') for the operating free stream velocity. The upper surface pressure measurement and 5-hole probe measurement were performed at 40 m/s.

Fig. 1 LEX/Delta wing model in the test section of the KAFA subsonic wind tunnel

The corresponding Reynolds number, based on the wing centerline chord(600 mm), was $Re_c = 1.76 \times 10^6$. The angle of attack, α, ranged from 10° to 40°, and the sideslip angle, β, ranged from 0° to −20°. The negative sideslip angle denotes that the central axis of the delta wing rotates in a clockwise direction against the free stream. Thus, the left wing is on the windward side, and the right wing is on the leeward side of the wing. Figure 1 shows the experimental model mounted in the wind tunnel test section.

The off-surface flow visualization was made in a smaller low-speed wind tunnel at the Korea Air Force Academy, a test section size of 0.9 m (W) ×0.9 m(H) ×2.1 m(L). The turbulence intensity was less than 0.2% for the available test section speeds (3.6~50 m/s). The free stream velocity of the off-surface flow visualization was 6.2 m/s, which corresponds to the Reynolds number of 1.82×10^5.

2.2 LEX/Delta wing model

As shown in Fig. 2, a flat LEX/delta wing with a sharp leading edge model was used in the present study. The sharp leading edge was obtained by beveling 25° from below, while leaving the upper surface flat. It has a 65° sweepback angle with a 600 mm root chord without LEX, and 795 mm with LEX. The length of span at the trailing edge is 475.4 mm, with a wing thickness of 15 mm. The LEX was also a flat plate 0.35 mm

thick with symmetrically beveled leading and side edges. The LEX had 65°/90° sweep angle. The apex portion of the pure delta wing could be removed and be replaced with the LEX. Thus, the model has the configuration of the delta wing having LEX.

The wing was instrumented with four spanwise rows of upper surface static pressure taps on the entire wing to investigate the effects of the sideslip angle. The pressure rows were located at 30%, 43%, 60%, and 80% of the distance along the wing centerline chord(c), measured from the wing apex. The number of pressure taps on each chord station was 47 along the entire span. Thus, a total of 188 pressure taps were used to collect time averaged surface pressure data. The pressure taps on each chord station were located at the same relative span position normalized by local semi-span(s).

The off-surface visualization data were obtained through a 2/3 reduced model, which has the same planform geometry and sharp leading edge as those of the model used in the wing upper surface pressure and 5-hole probe measurements.

In this study a model coordinate axis was used (Fig. 2). Thus, x is the coordinate along the wing centerline measured from the wing apex, y is the coordinate along the wing span measured from the wing centerline, and z is the coordinate normal to the wing upper surface.

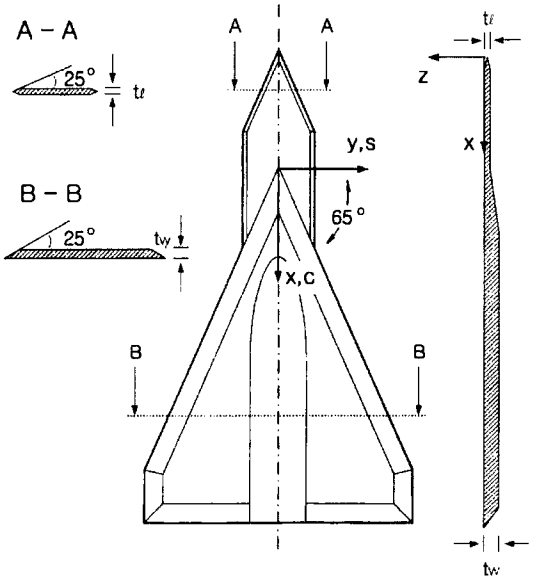

Fig. 2 Geometry of experimental model

2.3 Pressure and cross flow velocity measurement

The static pressure on the wing upper surface was obtained by using PSI 8400 pressure measuring system. The wing surface pressure data presented in this study was an ensemble average of 300 pressure signals of each pressure tap. The measured surface pressure data is accurate within 0.05%. The 5-hole probe (United Sensor SPA-12-6-45-C) was employed to measure total pressure and cross flow velocity vectors of the cross-section of the vortical flow. The 5-hole probe measurement data was also an ensemble average of 300 signals in the same way as the wing upper surface pressure measurement. The measuring section was normal to the wing surface. The axis of the probe was parallel to the wing surface and to the wing centerline chord. The calibration results showed that the 5-hole probe measured the velocity vector angle with an error of less than 3% for the pitch angle below 45°. The total pressure field of each vortical wake cross-section was represented by total pressure coefficient contours.

2.4 Visualization of vortical flow field

Micro water droplet and laser beam sheets were used for the off-surface flow visualization. The 5~10 μm sized water droplets were generated by a home-style ultrasonic humidifier. A 3 W Argon

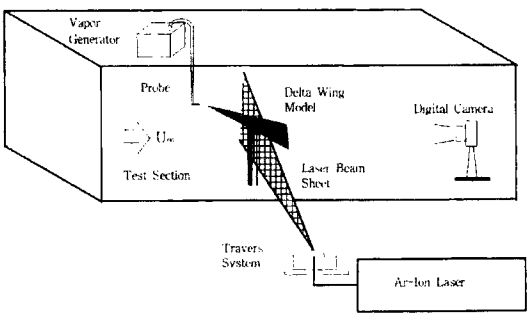

Fig. 3 Experimental set-up for off-surface visualization

ion laser was used to generate the laser light sheet. The laser light sheet was used to a interrogate specific cross section of the vortical wake. A cylindrical lens and convex focusing lens were used to form a laser light sheet, which was perpendicular to the wing surface. The illuminated planes were recorded on a high resolution digital camera (SONY DCR-VX 2000 NTSC). Other details of the flow visualization technique were described in Sohn & Lee(2002). Figure 3 shows the experimental setup of the visualization technique.

3. Discussion of Results

3.1 Overall vortical flow field

The prospective visualization results at several chordwise stations for various sideslip angles ($\beta=0°$, $-5°$, $-10°$, and $-15°$) are shown in Fig. 4. The perspective photos were obtained from dynamic images, which were taken by a camera positioned downstream of the wing trailing edge with a birds eye view, and a laser light sheet moving down stream with a constant speed.

In Fig. 4(a), the development of two distinct vortex pairs is observed on the front section of the wing for the zero sideslip angle. At the middle region of the wing, the vortices start to interact with each other, inter-wind, and eventually merge into one vortex at the rear part of the wing. At the sideslip angle of $-5°$(Fig. 4(b)), the inboard movement and expedited breakdown of the vortices are observed on the windward side.

Whereas, the coiling and breakdown of the wing and the LEX vortices are suppressed on the leeward side. At large sideslip angles, (Fig. 4(c, d)), the vortex breakdown position moves upstream region of the wing on the windward side. However, on the leeward side, the vortex pair remains distinguishable without breakdown over the entire chord station. This illustrates that the vortex breakdown is promoted on the windward side by sideslip, whereas the vortex breakdown is suppressed on the leeward side by sideslip.

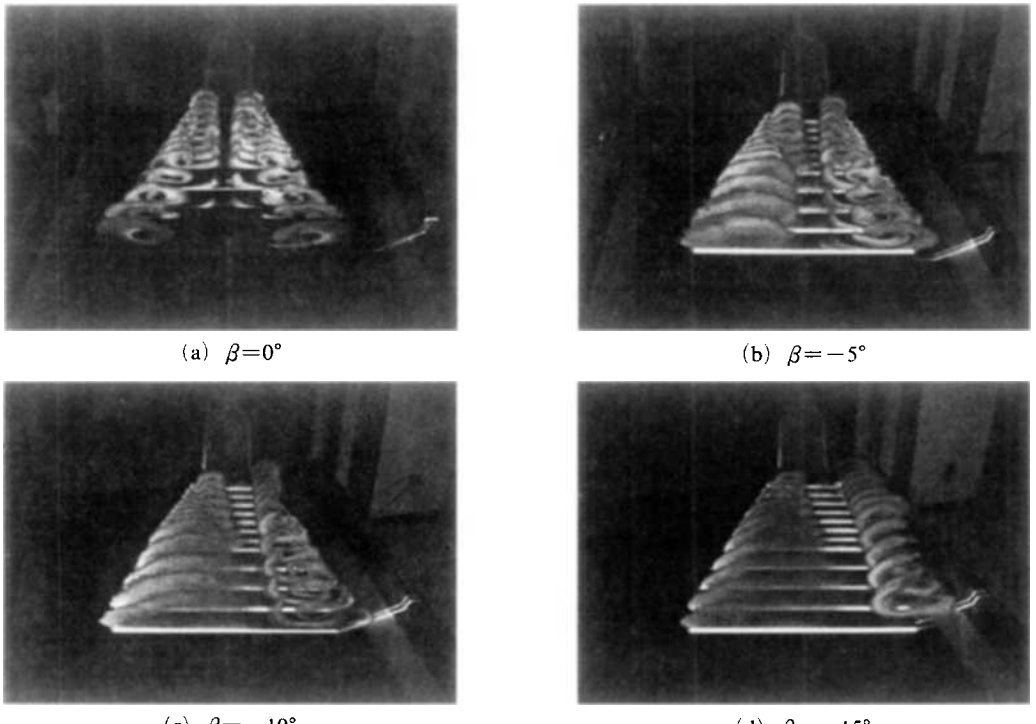

(a) $\beta=0°$ (b) $\beta=-5°$

(c) $\beta=-10°$ (d) $\beta=-15°$

Fig. 4 Perspective photos of the wake section at $\alpha=24°$

The flow visualization data on the vortex trajectory is shown in Fig. 5. The vortex core locations were visually selected from the photographs in a careful manner, and their coordinates were non-dimensionalized using the half span(s) for y and z coordinates. On the windward side, the wing vortex core moves inboard and away from the wing surface. The core of the LEX vortex enters the middle of the wing wake region, moving inboard and closer to the wing surface. At about middle region of the wing, x/c=0.43, these two vortices rotate clockwise, and coiling around each other. On the leeward side these vortices rotate in a counter clockwise direction, coiling each other through the last chord station. The crossover point of the interacting LEX and wing vortices moves upstream with increasing sideslip angle.

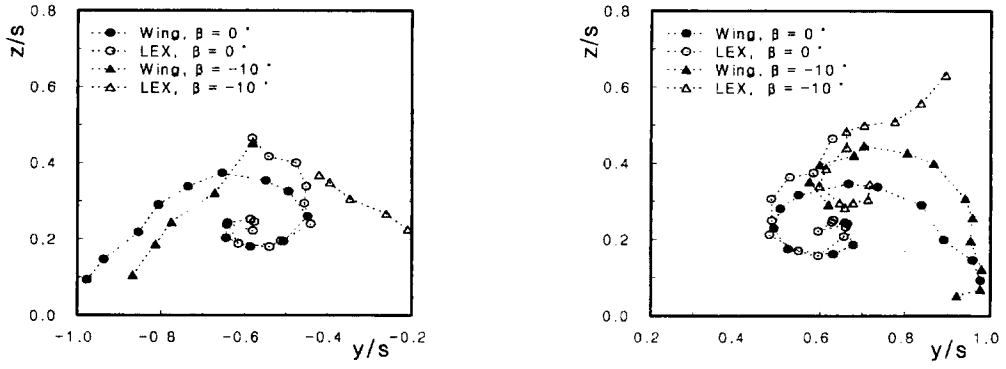

(a) Windward side (b) Leeward side

Fig. 5 Locus of vortex cores at different chord station (α=24°, β=−10°)

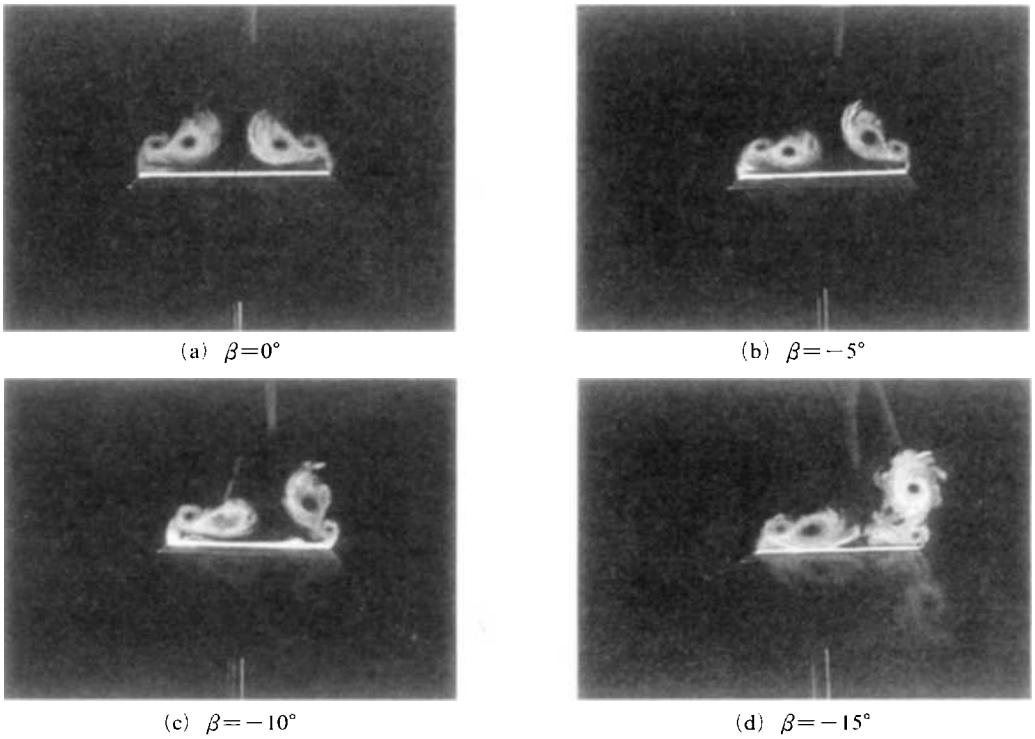

(a) β=0° (b) β=−5°

(c) β=−10° (d) β=−15°

Fig. 6 Effect of sideslip angle on the vortex structure at α=24°, and x/c=0.43

3.2 Detailed cross flow structure

Figure 6 presents the effects of the sideslip angle on the vortex structures at the middle region of the wing, x/c=0.43. The variation of the position and structure of the LEX and wing vortices can be observed. Considering the relative position of the vortex pairs on each side of the wing, the yaw effect on the mutual induction and the interaction of the LEX and wing vortices can be illustrated. On the windward side, the LEX vortex core and wing vortex core are almost parallel to the wing surface with increasing sideslip angle. However, on the leeward side, as sideslip angle increases, the relative position of LEX vortex to wing vortex changes from a horizontal to a vertical position. Thus, the yaw angle delays the interaction of vortices on the leeward side.

As the sideslip angle increases (Fig. 6(b)), visualization data reveals a system of co-rotating vortical structures around the LEX core vortex on the leeward side of the wing. This co-rotating sub-vortices structural feature, which is expected to undergo transition to turbulence, is significant at $\beta=-15°$(Fig. 6(d)). This unsteady vortical structure, which rotate around the LEX vortex, resembles the spanwise vortical structures found in a two-dimensional mixing layer downstream of a splitter plate (Winant and Browand, 1974). The cause of this type of sub-vortices was assumed to be a local three-dimensional Kelvin-Helmholtz instability of the free shear layer (Ozgoren et al., 2002; Riley and Lowson, 1998; Menke and Gursul, 1997). These structural features co-rotating sub-vortices disappear with further increase of the angle of attack (not shown in Figures).

The effect of the angle of attack on the behavior of the vortical flow at the same sideslip condition can be seen in Fig. 7. It is observed that the visualization results at the four different angles of attack have a somewhat similar pattern in vortical structure, but have slightly different vortical strength and vortex core locations. It can also be observed the higher the angle of attack is, the larger the diameter of black dot, which denotes

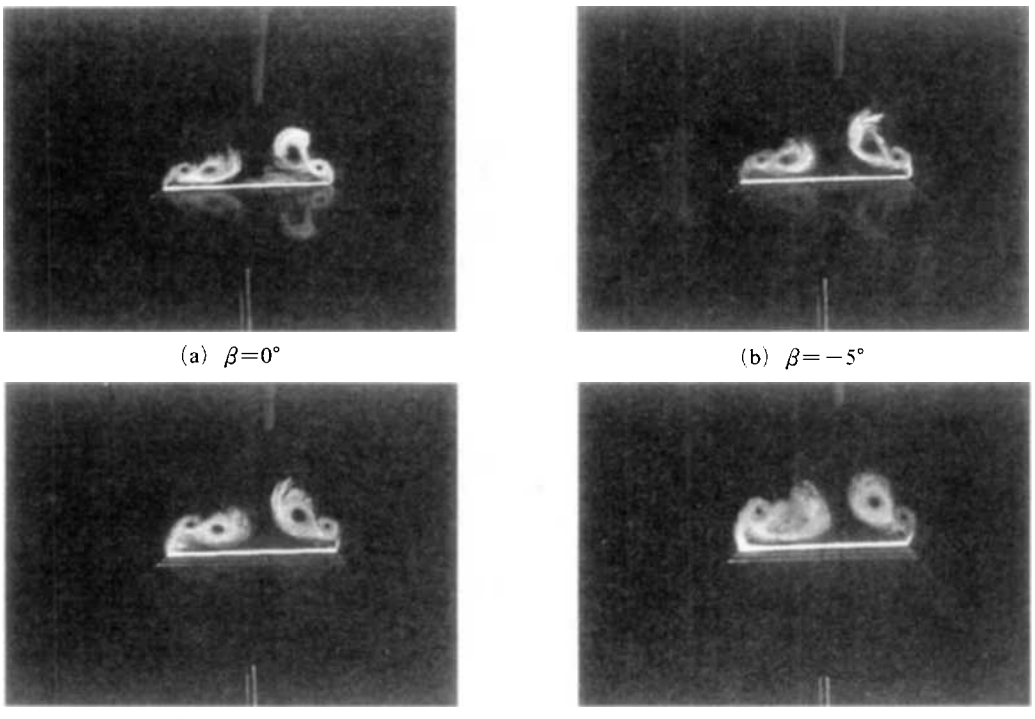

(a) $\beta=0°$ (b) $\beta=-5°$

(c) $\beta=-10°$ (d) $\beta=-15°$

Fig. 7 Effect of angle of attack on the vortex stucture at $\beta=-5°$, and x/c=0.43

the rate of concentration of vortices is. As the angle of attack increases, the inner LEX vortex moves downward and outboard, and the outer wing vortex moves upward and inboard on the windward side of the wings. Whereas, both the LEX and wing vortex move upward and outboard on the leeward side. This shift of the vortex core position is more significant at large sideslip angles. At the angle of attack, $\alpha=28°$(Fig. 7(d)), the LEX vortex starts to break down on the windward side. This is because the wing vortex is continuously fed with vortices from the wing leading edge as well as from the shear layer between the wing and LEX vortices. Whereas, the vorticity fed into the LEX vortex gradually diminishes downstream of the wing. Vortex interaction and breakdown is enhanced on the windward side at higher angle of attack, especially at larger sideslip condition.

Both total pressure coefficient contour plot and cross flow velocity are also good indicators of the presence of vortices. The total pressure coefficient, $C_{pt}=(P_t-P_\infty)/q_\infty$, is defined as the difference between local total pressure(P_t) and free-stream total pressure(P_∞), and normalized by free-stream dynamic pressure(q_∞). Thus, the total pressure coefficient means the total pressure loss coefficient.

Figure 8 shows the vortical wake section of the delta wing with LEX configuration for a sideslip angle of 10° and angle of attack of 24°, represented by a total pressure contour and cross flow velocity vector. This transverse plane total pressure distribution and cross flow velocity illustrate the vortex interaction and breakdown in more detail. On each side of the wing, development of the two vortices was observed, one from the LEX, and the other from the wing leading edge in Fig. 8(a). On the windward side, the LEX vortex enters the wing wake region more inboard and closer to the wing surface, while the leeward side LEX vortex enters wing wake region more outboard and farther from the wing surface. The LEX vortex starts to merge with the wing vortex at the middle region of the wing (x/c=0.6) on the windward side. The merging of these vortices is distinguished by the coalescence of the two distinct low total pressure zones. Toward the rear of the wing, these merged vortices undergo vortex breakdown as shown in Fig. 8(d). the vortex breakdown produces a substantial increase in the magnitude of the total pressure loss and distributes this loss over a larger area as shown at the downstream station in Fig. 8(b). While on the leeward side, the LEX vortex moves further outboard of the wing by sideslip. The wing vortex

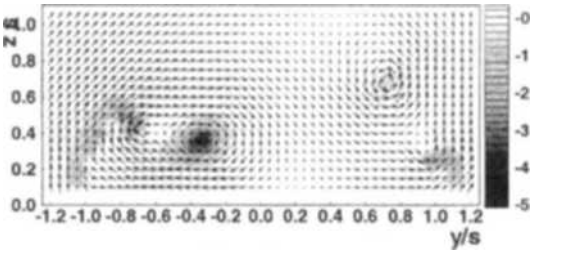

(a) x/c=0.3

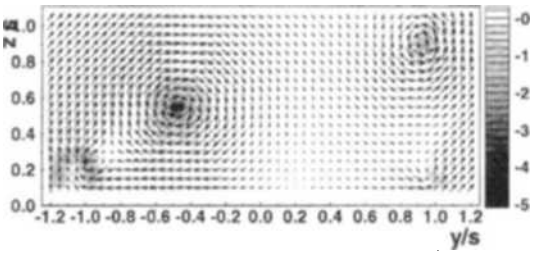

(b) x/c=0.43

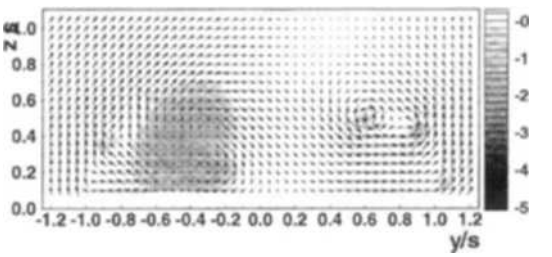

(c) x/c=0.6

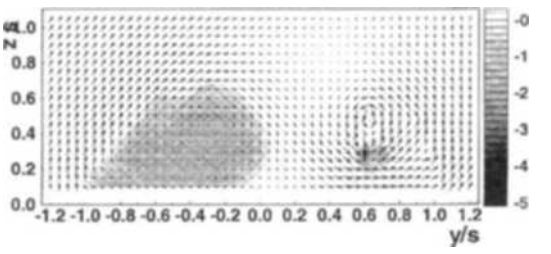

(d) x/c=0.48

Fig. 8 Total pressure contour and cross flow velocity of the wake section at $\alpha=24°$ and $\beta=-10°$

also moves slightly farther outboard and becomes weak. As a result, the vortex breakdown does not occur, and the vortex cores maintain their identities without merging into a single vortex.

For sideslip condition, a stronger vortex is formed on the portside. For example, at x/c=0.3, the total pressure coefficient of the LEX core was −4.5 and that of the wing vortex core was −5.1 on the portside. However, on the starboard side, the total pressure coefficients of the LEX and the wing vortex cores were −2.4 and −0.9 respectively. The strength of the wing vortex increases with increasing downstream distance of the wing apex. As the strength of the wing vortex increases, the weaker LEX vortex is drawn downward because of the velocity field induced by the wing vortex. At the downstream station, the LEX vortex is observed to merge with the wing vortex.

3.3 Aerodynamic load characteristics

The upper wing surface pressure distribution, in Fig. 9, illustrates the combined effects of angle of attack and sideslip on the aerodynamic load characteristics of the model. Figure 9 shows spanwise suction pressure distributions at 30%, 43 %, 60, and 80% chord stations from wing apex. This shows that the sideslip angle significantly changes the upper wing surface pressure distribution, especially at a higher angle of attack.

At a medium angle of attack, $\alpha=24°$(Fig. 9 (a)), the pressure distribution of the two sides of the wing are similar to each other in shape, but they are different in the magnitude of the suction pressure peak. The suction pressure peak of the windward side is greater in magnitude than that of the leeward side. For the small sideslip angle ($\beta=-5°$), the suction pressure distribution with the distinct peaks is preserved even at the rear part of the wing. However, delta wing alone configuration, the pressure distribution rapidly collapsed, that means onset of vortex breakdown, at the middle region of the wing for the same condition, $\alpha=24°$ and $\beta=-5°$(Lee and Sohn, 2003). This also demonstrates that the beneficial interaction of the LEX and the wing vortex is preserved at small sideslip condition, $\beta=-5°$. However, greater than this sideslip angle, the suction pressure distribution collapses either at the rear part of the wing.

At a relative high angle of attack, $\alpha=36°$(Fig. 9(b)), the suction pressure peak increases on the windward side and decreases on the leeward side as the sideslip angle increases in magnitude. The spiked suction pressure distribution on the windward side is completely destroyed for more than the sideslip angle of −10° at the rear part of the wing. The suction pressure of each side of the

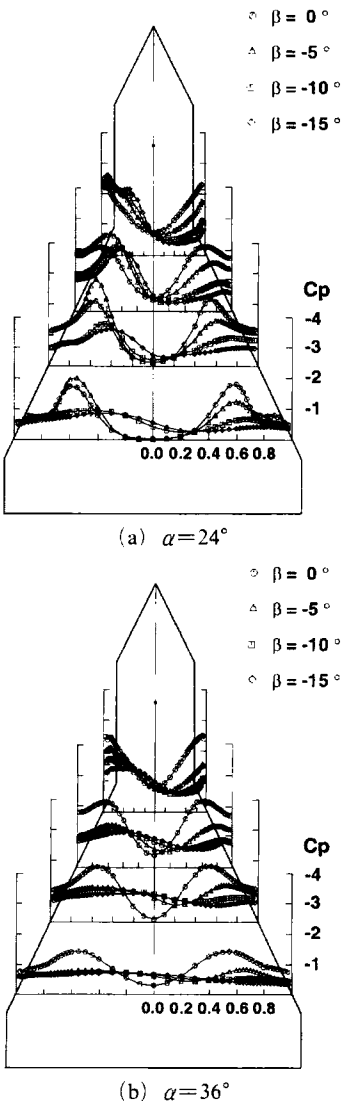

(a) $\alpha=24°$

(b) $\alpha=36°$

Fig. 9 Effect of sideslip angle on the upper wing surface pressure distribution

wing decreases rapidly at all chord stations with an increasing sideslip angle. At a larger sideslip angle, this collapse of the suction pressure on the both side of the wing is typical of vortex breakdown. At higher angle of attack, no more vortex lift is expected even for small sideslip angles because of vortex breakdown on the windward side and lift-off of vortices from the wing surface on the leeward side. Asymmetry of the spanwise pressure distribution of the two sides of the wing becomes apparent with increased angle of attack and sideslip angle.

Figure 10 shows the variation of the suction pressure peak with the angle of attack for different sideslip angles. In Fig. 10, W denotes the windward side and L denotes the leeward side. Except for a small sideslip angle, $\beta=-5$℃, the tendency of the peak value variation with angle of attack is very similar each other. At a small sideslip angle, the suction pressure peak of windward side increases in the magnitude of 3.5 at 60% chord station as the angle of attack increases up to $\alpha=30°$, after which decrease. At a larger sideslip angle, $\beta=-10°\sim-20°$, the suction pressure peak of windward side become much weaker($C_{pmax}=2.85\sim2.38$ at x/c=0.6) than that of smaller sideslip angle. This indicated that the sideslip make vortex breakdown promote on the windward side.

Whereas, on the leeward side, the value of suction pressure peak increased monotonically with the angle of attack for the entire region of the wing. This increment of the vortex strength implies the delay or suppress of the vortex breakdown up to a high angle of attack on the leeward side.

For smaller sideslip angle, $\beta=-5°$, the pattern of peak value variation with the angle of attack is slightly different from larger sideslip condition. The magnitude of the peak value is much higher than that of the larger sideslip, and the angle of attack where the peak value occurs, is also much higher. In particular, at the middle region of the wing(Fig. 10(c)), the peak value of the windward side ($C_{pmax}=1.0\sim1.18$) was smaller than that of the leeward side ($C_{pmax}=1.55\sim1.20$) for the angles of the attack of $32°\sim36°$. This result was not observed for other ranges of angles of attack and sideslip angles. At this range of angle of attack and sideslip angles, a negative rolling moment would be expected. For the delta wing alone configuration, this negative rolling moment, rolling moment reversal, occurred relatively broad ranges of angle of attack and sideslip angle, $\alpha=24°\sim36°$ and $\beta=-5°\sim-15°$(Lee and Sohn, 2003). Thus, compare to the delta wing only configuration, much limited rolling moment reversal ranges of angle of attack and sideslip angle also reveals a beneficial effect of LEX on the stabilization of vortical flow field.

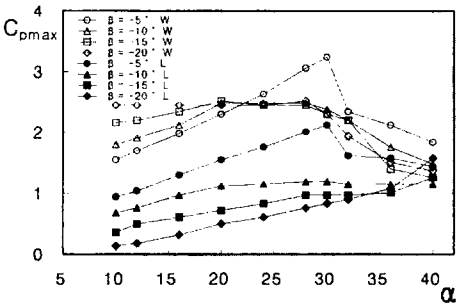

(a) x/c=0.3

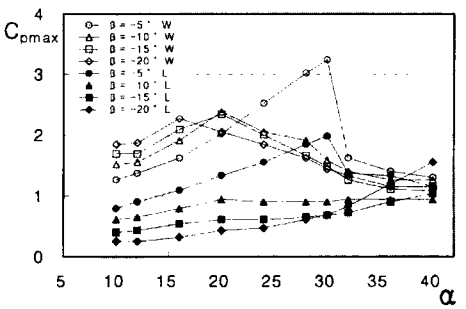

(b) x/c=0.43

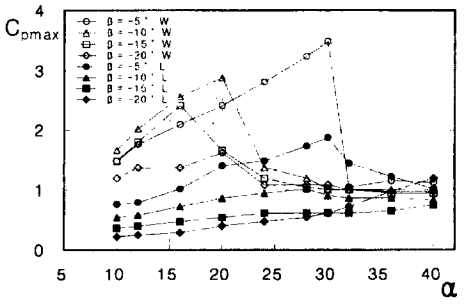

(c) x/c=0.6

Fig. 10 Suction peak variation with the angle of attack and the sideslip angle

4. Conclusions

In this article, the effects of angle of attack and sideslip on the vortical flow of LEX/delta wing configuration were analyzed. Compare to the delta wing alone configuration, the experimental data has clearly shows that the beneficial effect of the LEX vortex on the vortical flow field, even at a higher angle of attack for small sideslip angle. The LEX vortex stabilized the wing vortical flow field to delay the breakdown up to $4°\sim6°$ of angles of attack in non-zero sideslip condition.

The interaction between LEX and wing vortices was highly sensitive to sideslip. With sideslip angle, the interaction and the breakdown of the LEX and wing vortices were promoted on the windward side, whereas, they were suppressed on the leeward side. The vortex breakdown on the windward side was characterized by a forward movement toward the apex of the model as the angle of attack and the sideslip angle were increased. On the leeward side, the LEX and the wing vortices coiled each other while keeping their identities even at a higher angle of attack and sideslip angle. The rolling moment reversal would be expected much limited conditions of angle of attack and sideslip angles($\alpha=32°\sim36°$ for $\beta-5°$).

Acknowledgment

This research was sponsored by the Korea Science and Engineering Foundation (Grant Number KOSEF R01-2000-000-0318-0). The authors would like to thank KOSEF.

References

Boer, R. G. and Cunningham, A. M., 1990, "Low-Speed Unsteady Aerodynamics of a Pitching Straked Wing at High Incidence- Part I: Test Program," *J. of Aircraft*, Vol. 27, No. 1, pp. 23~30.

Chung, J., Cho, T., Lee, J. and Sung, B., "Wind Tunnel Test of a Canard Airplane," *KSME International Journal*, Vol. 16, No. 1, pp. 12~131.

Cornelius, K. C., 1995, "Analysis of Vortex Bursting Utilizing 3-D Laser Measurements," *J. of Aircraft*, Vol. 32, No. 2, pp. 297~306.

Cunningham, A. M. and Boer, R. G., 1990, "Low-Speed Unsteady Aerodynamics of a Pitching Straked Wing at High Incidence- Part I: Harmonic Analysis," *J. of Aircraft*, Vol. 27, No. 1, pp. 31~41.

Ericksson, L. E., 1999, "Vortex Characteristics of Pitching Double-Delta Wing," *J. of Aircraft*, Vol. 36, No. 2, pp. 349~356.

Ekaterinaris, J. A., Coutley, R. L., Schiff, L. B. and Platzer, M. F., 1995, "Numerical Investigation of Incidence Flow over a Double-Delta Wing," *J. of Aircraft*, Vol. 32, No. 3, pp. 457~463.

Fujii, K. and Schiff, L. B., 1989, "Numerical Simulation of Vortical Flows over a Strake-Delta Wing," *AIAA J.*, Vol. 27, No. 9, pp. 1153~1162.

Grismer, D. S. and Nelson, R. C., 1995, "Double Delta-Wing Aerodynamics for Pitching Motions With and Without Sideslip," *J. of Aircraft*, Vol. 32, No. 6, pp. 1303~1311.

Hebber, S. K., Platzer, M. F. and Fritzelas, A. E., 2002, "Reynolds Number Effects on the Vortical-Flow Structure Generated by a Double-Delta Wing," *Experiments in Fluids*, Vol. 28, pp. 206~216.

Hoeijmarkers, H. W. M. and Vaatstra, W., 1983, "Vortex Flow over Delta and Double Delta Wing," *J. of Aircraft*, Vol. 20, No. 9, pp. 825~832.

Lee, K. Y., and Sohn, M. H., 2003, "Combined Effects of Sideslip and Angle of Attack on the Vortical Flow of Delta Wing," *Journal of Korean Society of Aeronautical & Space Science*, Vol. 31, No. 2, pp. 17~24.

Menke, M. and Gursul, I., 1997, "Unsteady Nature of Leading Edge Vortices," *Physics Fluids*, Vol. 9, No. 10, pp. 2960~2966.

Ozgoren, M., Sahin, B. and Rockwell, 2002, "Vortex Structure on a Delta Wing at High Angle of attack," *AIAA J.*, Vol. 40, No. 2, pp. 285~292.

Riley, A. J. and Lowson, M. V., 1998, "Development of a Three-Dimensional Free Shear La-

yer," *J. Fluid Mechanics*, Vol. 369, pp. 49~89.

Sohn, M. H. and Lee, K. Y., 2002, "Experimental Investigation of Vortex Flow of a Yawed Delta Wing Having Leading Edge Extension," *AIAA Paper*, pp. 2002~3267.

Verhaagen, N. G., 1999, "Effects of Reynolds Number on the Flow over 76/40-deg Double-Delta Wings," *AIAA Paper*, pp. 142~152.

Verhaagen, N. G. and Naarding, S. H. J., 1989, "Experimental and Numerical Investigation of the Vortex Flow over a Yawed Delta Wing," *J. of Aircraft*, Vol. 26, No. 11, pp. 971~978.

Winant, C. D. and Browand, F. K., 1974, "Vortex Pairing: The Mechanism of Turbulent Mixing-Layer Growth at Moderate Reynolds Number," *J. Fluid Mechanics*, Vol. 63, pp. 237~255.